Evolution of the superconducting properties in $FeSe_{1-x}S_x$

S. A. Moore,[1] J. L. Curtis,[2] C. Di Giorgio,[1,*] E. Lechner,[1] M. Abdel-Hafiez,[3] O. S. Volkova,[4,5,6] A. N. Vasiliev,[4,5,6] D. A. Chareev,[5,7] G. Karapetrov,[2] and M. Iavarone[1]

[1]*Department of Physics, Temple University, Philadelphia, Pennsylvania 19122, USA*
[2]*Department of Physics, Drexel University, Philadelphia, Pennsylvania 19104, USA*
[3]*Center for High Pressure Science and Technology Advanced Research, Shanghai, 201203, China*
[4]*Physics Faculty, M.V. Lomonosov Moscow State University, Moscow 119991, Russia*
[5]*Theoretical Physics and Applied Mathematics Department, Ural Federal University, 620002 Ekaterinburg, Russia*
[6]*National University of Science and Technology "MISiS," Moscow 119049, Russia*
[7]*Institute of Experimental Mineralogy, Russian Academy of Sciences, 142432 Chernogolovka, Moscow District, Russia*

(Received 31 August 2015; revised manuscript received 13 October 2015; published 7 December 2015)

We present scanning tunneling microscopy and spectroscopy measurements on $FeSe_{1-x}S_x$ single crystals with $x = 0$, 0.04, and 0.09. The S substitution into the Se site is equivalent to a positive chemical pressure, since S and Se have the same valence and S has a smaller ionic radius than Se. The subsequent changes in the electronic structure of FeSe induce a decrease of the structural transition temperature and a small increase in the superconducting critical temperature. The evolution of the gaps with increasing S concentration suggests an increase of the hole Fermi surface. Moreover, the vortex core anisotropy, that likely reflects the Fermi surface anisotropy, is strongly suppressed by the S substitution.

DOI: 10.1103/PhysRevB.92.235113 PACS number(s): 74.70.Xa, 74.25.Jb, 74.55.+v, 74.25.F−

I. INTRODUCTION

FeSe has the simplest crystallographic structure among the family of iron-based superconductors and investigations into this system may yield a better understanding of the origin of superconductivity in iron pnictides/chalcogenides. FeSe undergoes a structural phase transition from tetragonal to orthorhombic at $T_s \approx 90$ K, but differently from other Fe-based superconductors this is not accompanied by a transition to a long-range magnetic order phase [1]. Below T_s a strong electronic anisotropy develops that is detected through an anisotropic Fermi surface, an anisotropic resistivity, and is sensitive to external parameters such as in-plane strain [2]. The dramatic changes in the electronic properties cannot be explained in terms of the small changes in the lattice parameters of the order of 0.1%; therefore, this phase is driven by an electronic degree of freedom, namely the electronic nematic order [3]. This *C4* symmetry breaking, which breaks the rotational symmetry without changing the translational symmetry of the lattice, may play an important role in understanding the superconducting state that sets in below $T_c = 8.5$ K [4]. In Fe-based superconductors, the nematic phase is usually regarded as the orthorombic phase sandwiched between the structural transition and the onset of the long-range magnetic order. However, in the case of FeSe no long-range magnetic order has been observed, which makes FeSe an ideal system for the study of the nematic order even in the superconducting state. Indeed, the strong Abrikosov vortex core anisotropy observed in FeSe [5] has been regarded as a manifestation of the nematic order in this material [6,7].

The origin of the nematicity in Fe-based superconductors is still a subject of intense debate. It has been proposed that nematicity could be driven either by orbital ordering of the Fe *d* electrons or by spin fluctuations. Furthermore, orbital order with *interorbital* electron-electron interactions would favor a sign preserving *s*-wave superconducting order parameter [8,9], while spin fluctuations with strong *intraorbital* interaction would favor a sign-changing $s_{\pm}$-wave or *d*-wave pairing [3,10–17]. The experimental findings in Fe-based superconductors so far have supported the latter scenario [18,19]. However, the absence of long-range magnetic order in FeSe has challenged this explanation for this compound. ARPES measurements have found evidence of a large band splitting caused by orbital ordering [2,20,21] that seems to point toward an electronically driven transition in FeSe.

Recent advances in single crystal growth and availability of large size high quality single crystals [22,23] have allowed neutron scattering studies that revealed the presence of magnetic stripe fluctuations coupled with the orthorombicity and the presence of a resonant mode in the superconducting state at about 4 meV [24] reflecting the importance of magnetic fluctuations in the superconducting state.

Differently from other Fe-based superconductors, the Fermi surface of FeSe consists of one hole pocket at the Γ point, while a second Γ band is pushed below the Fermi level by 50 meV [2,25,26]. There exist possibly two degenerate electron pockets at the Brillouin zone corners (*M* point) [2,25]. The resulting Fermi surface is much smaller than that predicted from DFT calculations and has carrier densities of $n_h = 0.015$ carriers/Fe and $n_e = 0.0093$ carriers/Fe [27].

Tunneling spectroscopy experiments have been performed by scanning tunneling spectroscopy on thin films [5] and single crystals [28] and by planar junctions on thin films [29]. Gap values have also been extracted from point contact spectroscopy [30] and specific heat experiments on single crystals [31]. Many features have been detected in the low excitation energy spectrum, but their interpretation remains controversial. A spectral feature at about 2.4 meV has been reported in all tunneling experiments, which has been

*Permanent address: E.R. Caianiello Physics Department and NANOMATES, Research Centre for Nanomaterials and Nanotechnology, University of Salerno, Fisciano (SA), Italy.

interpreted as one of the superconducting gaps in the excitation spectrum. At least two more features have also been observed. A smaller feature at an energy on the order of 1 meV in point contact spectroscopy experiments has been interpreted as another gap, while a high energy feature at about 3.5 meV has been interpreted as a boson mode in some reports [32] and as a gap feature in others [28].

Here, we report scanning tunneling microscopy and spectroscopy measurements of $FeSe_{1-x}S_x$ single crystals. The substitution of S has an effect equivalent to a positive chemical pressure since S and Se have the same valence and S has a smaller ionic radius than Se. The samples studied show an increase of the superconducting temperature for all substitution levels considered in this study and a corresponding decrease of the temperature at which the structural transition occurs. Our results indicate changes in the electronic structure of this material with S substitution and suggest a reduction of the Fermi surface anisotropy. Moreover, the in-gap resonant states at the impurity sites strongly support a nodal order parameter, which implies the importance of the magnetic fluctuations scenario assisting the superconducting pairing in this compound.

II. SAMPLE CHARACTERIZATION

$FeSe_{1-x}S_x$ single crystals were grown in evacuated quartz ampoules using the AlCl3/KCl flux technique in a temperature gradient (from 400 °C to ∼50 °C) for 45 days [22]. The chemical composition of crystals was studied with a digital scanning electron microscope TESCAN Vega II XMU [22]. The standard deviation of the average S concentration gives an indication of the homogeneity of S within the crystals. Therefore, the composition and in particular the S-concentration level was obtained by averaging over several different points of each single crystal. The analysis showed that the approximate chemical compositions are $FeSe_{1-\delta}$ ($x = 0$), $Fe(Se_{0.96\pm0.01}S_{0.04\pm0.01})_{1-\delta}$ ($x = 0.04$), and $Fe(Se_{0.91\pm0.01}S_{0.09\pm0.01})_{1-\delta}$ ($x = 0.09$).

The crystals have a platelike shape with the c axis oriented perpendicular to the crystal plane with only the tetragonal β-FeSe phase present. The lattice parameters $c = (5.52 \pm 0.01)$ Å and $a = (3.77 \pm 0.01)$ Å were found via x-ray diffraction for FeSe single crystals ($x = 0$). X-ray diffraction shows a small decrease in the lattice parameter c with S substitution to $c = (5.50 \pm 0.01)$ Å in the $FeSe_{0.91}S_{0.09}$ samples.

Resistivity measurements were performed by standard four-probe alternating current dc method with the current applied parallel to the *ab* plane. Electrical contacts parallel to the *ab* plane were made using thin copper wires attached to the sample with silver epoxy. High field resistivity measurements were done using a superconducting magnet up to 21 T manufactured by Cryogenic Ltd. The main panel of Fig. 1 shows the temperature dependence of the resistivity. The superconducting critical temperatures are 8.5 K, 9.6 K, 10.1 K for $x = 0, 0.04, 0.09$, respectively. The two insets of Fig. 1 show the evolution of the superconducting transition in the presence of an applied magnetic field perpendicular to the *ab* plane (up to 9 T). Negligible smearing of the superconducting transition indicates high quality samples. A kink in the resistivity curves is present at the structural phase

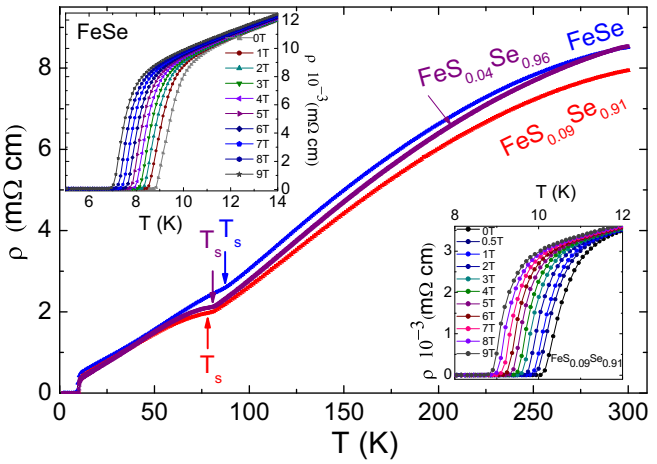

FIG. 1. (Color online) Temperature dependence of the in-plane resistivity of FeSe (blue curve) and $FeSe_{1-x}S_x$ single crystals with $x = 0.04$ (purple curve) and $x = 0.09$ (red curve). The arrows indicate the temperature T_s at which the tetragonal-to-orthorhombic structural transition occurs. The two insets show the evolution of the superconducting transition in magnetic fields, up to 9 T, applied along the c axis.

transition from tetragonal to orthorhombic. This transition temperature T_s decreases from ≈ 90 K in the sample with $x = 0$ to ≈ 80 K in the sample with $x = 0.09$. At temperatures above the structural transition we observe a decrease of the in-plane resistivity as a function of the S substitution. These results are very similar to the results reported for the in-plane resistivity of FeSe single crystals under helium pressure [33]. In the case of pressure studies the initial increase in the superconducting temperature is close to $dT_c/dP = (5.8 \pm 0.1)$ K/GPa. Therefore, an increase of T_c by 1.6 K for an S-substitution level of 9% would seem to be equivalent to a pressure of $P \approx 0.28$ GPa. This is also consistent with the corresponding decrease of the structural transition temperature of $dT_s/dP = -(31 \pm 0.7)$ K/GPa, that would give a decrease of ≈ 9 K for a pressure of ≈ 0.28 GPa, consistent with what we observe in the case of 9% S substitution. However, the reduction of the in-plane resistivity by $\Delta R/R \approx -13.6\%$, that we observe at 100 K in the 9% S substituted sample, seems to correspond to a higher equivalent hydrostatic pressure if we consider that in the case of pressure studies the reduction reported is $\Delta R(100\text{ K})/(R(100\text{ K})\Delta P) = -(22 \pm 1)\%$ GPa [33]. This seems to suggest that S substitution is not simply equivalent to applying of hydrostatic pressure.

III. SCANNING TUNNELING MICROSCOPY AND SPECTROSCOPY OF $FeSe_{1-x}S_x$ SINGLE CRYSTALS

Low temperature scanning tunneling microscopy (STM) and spectroscopy (STS) have been performed at $T = 400$ mK, $T = 1.5$ K, and $T = 4.2$ K using Unisoku UHV STM system, with a base pressure of 4×10^{-11} Torr. The samples were cleaved in UHV at room temperature and soon after were transferred to the STM at low temperature. Pt-Ir tips were used in all of our experiments, therefore the tunneling conductance between a normal electrode (tip) and a sample provides, in the

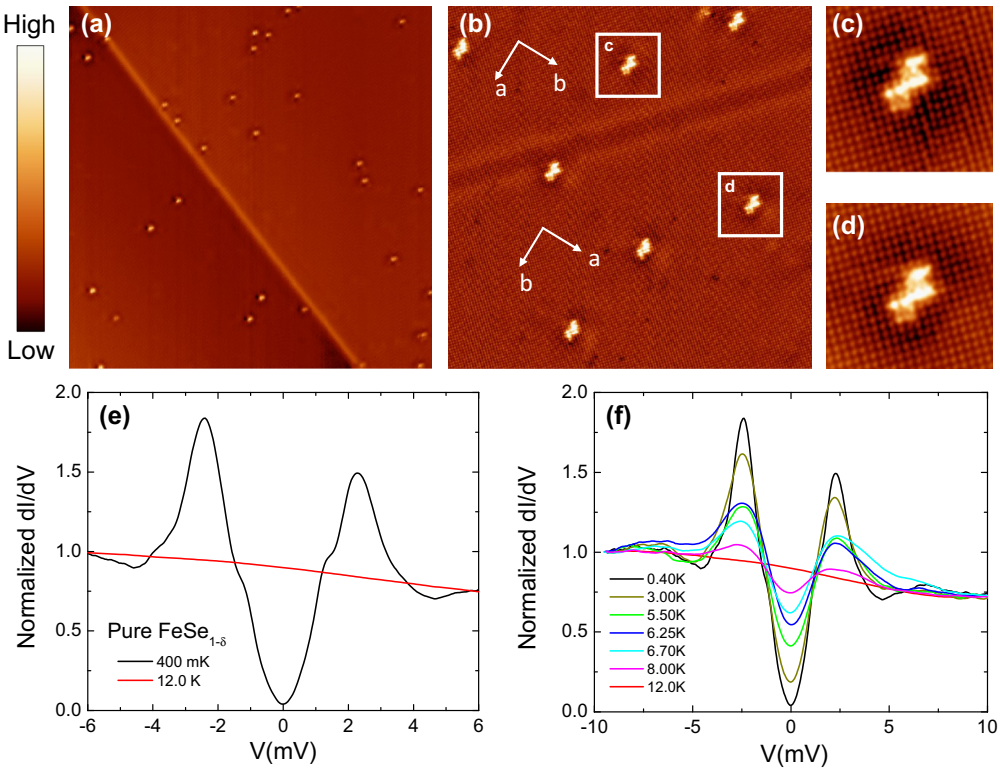

FIG. 2. (Color online) (a) Constant-current STM image of a cleaved (001) FeSe single crystal showing a twin boundary running from top left to bottom right. The scan area is 156 nm × 156 nm. Scanning parameters are $V = +25$ mV and $I = 50$ pA. (b) Zoomed in STM image of the twin boundary. Scan area is 50 nm × 50 nm. Scanning parameters are $V = +70$ mV and $I = 100$ pA. Crystallographic axes parallel to the Fe-Fe direction are shown with white arrows. The white squares indicate the two defects on both sides of the twin boundary shown in detail in (c) and (d). (c),(d) Atomic resolution STM topographic images of two defects. Scan areas are 7.5 nm × 7.5 nm. (e) Tunneling spectra dI/dV acquired far from defects and twin boundary on the surface of FeSe single crystals at $T = 0.4$ K (black curve), $T = 12$ K (red curve), and $H = 0$. (f) Evolution of the tunneling spectrum as a function of temperature from $T = 0.4$ K up to $T = 12$ K. For all spectra in this figure tunneling conditions are $V = -10$ mV, $I = 100$ pA; the modulation of the lock-in is $V_{\text{mod}} = 0.2$ mV. All spectra have been normalized to the value of the conductance at $V = -10$ meV.

limit of low voltages, the electronic density of states of the sample.

Atomically resolved images were acquired in the constant-current mode. Figure 2(a) shows a 156×156 nm^2 STM topography image acquired at the surface of a pure FeSe single crystal at $T = 1.5$ K. The image shows a large atomically flat surface with a very small amount of defects on the order of 0.001 defects/nm^2. The image also shows a line running across the surface at 45° with respect to the topmost Se lattice (along the Fe lattice), which represents a twin boundary. The appearance of the twin boundary in STM images is energy dependent; indeed at lower bias [Fig. 2(a)] it appears like a step, while at higher energy [Fig. 2(b)] it appears like a groove with an apparent corrugation of ≈7 pm consistent with previous reports [32,34]. This suggests that the apparent height of the twin boundary in STM images is primarily associated with electronic properties rather than actual topography. A zoomed-in image of defects on both sides of the twin boundary [Fig. 2(c) and Fig. 2(d)] shows that the dark features surrounding a defect are rotated by $\pi/2$ across the twin boundary as previously reported in thin films [32] and single crystals [34].

Conductance spectra (dI/dV), which are proportional to the local electronic density of states, have been acquired using the lock-in ac modulation technique while the I-V curves were recorded simultaneously. Figure 2(e) shows two tunneling spectra acquired at $T = 0.4$ K and $T = 12$ K on a single crystal with $x = 0$. The spectrum at low temperature is V-shaped in the low energy range, indicating the presence of nodes in the gap consistent with what has been reported in thin films [5] and single crystals [28]. There are clear coherence peaks in the spectrum at $\Delta = \pm 2.3$ meV that have been observed in other STM measurements both on thin films [5,32] and on single crystals [28,34], as well as in tunneling spectroscopy with planar junctions [29]. These peaks can be tracked in the temperature evolution of the tunneling spectra and they vanish at the bulk T_c of 8.5 K as shown in Fig. 2(f). These values of Δ and T_c yield $2\Delta/k_B T_c = 6.3$, which is much larger than the values of 3.53 and 4.3 predicted by the BCS theory for weak-coupling s wave and d wave, respectively, and places this system in the strong coupling limit. However, it is important to note that STM sensitivity is exponentially suppressed with increased in-plane momentum [35–37]; therefore, the main coherence peaks observed in all STM spectra are likely associated to the hole Γ band gap, while the tunneling matrix element for the M pocket should be reduced for c-axis tunneling. Other than these coherence peaks there are additional features in the observed tunneling

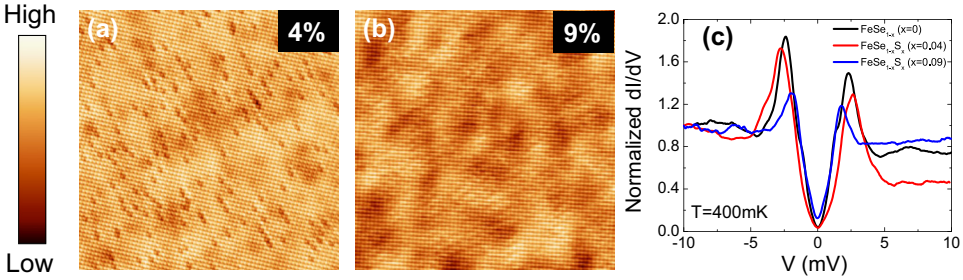

FIG. 3. (Color online) (a) Constant-current STM image of a cleaved (001) $FeSe_{0.96}S_{0.04}$ showing dark spots associated to the S substitution. Scan area is 25 nm × 25 nm. Scanning parameters are $V = 10$ mV and $I = 100$ pA. (b) Constant-current STM image of a cleaved (001) $FeSe_{0.91}S_{0.09}$ crystal. Scan area is 25 nm × 25 nm. Scanning parameters are $V = 10$ mV and $I = 100$ pA. (c) Tunneling spectra dI/dV acquired at $T = 400$ mK far from defects on the samples with $x = 0$ (black curve), $x = 0.04$ (red curve), and $x = 0.09$ (blue curve). Tunneling conditions are the same for all curves: $V = -10$ mV, $I = 100$ pA, and the lock-in modulation $V_{\text{mod}} = 0.2$ mV. The tunneling spectra have been normalized to the value of the conductance at $V = -10$ meV.

spectrum at 0.4 K, such as shoulders that appear symmetrically at around ±3.5 meV, which have been associated with a possible second gap [28]. However, these features can also be part of the electronic density of states redistribution associated with the boson mode in strongly coupled superconductors [38]. Another pair of shoulders also appears in our tunneling spectra symmetrically at $\approx \pm 1.4$ meV. We have observed these features in tunneling spectra acquired more than 30 nm away from any defect or twin boundary excluding the possibility that they could be associated with resonances at impurity sites, which normally decay within about 10 nm as shown in the following section.

It should also be noted that the tunneling spectra have an asymmetric background for occupied and unoccupied states which is quite likely associated to the band structure in this material [38].

In Figs. 3(a) and 3(b) we report the STM topography acquired on samples S substituted with $x = 0.04$ and $x = 0.09$, respectively. Dark spots are associated with the S as the density corresponds closely to the nominal concentration of the sample measured. In Fig. 3(c) we show the evolution of the tunneling spectra at $T = 0.4$ K for the $x = 0$, 0.04, and 0.09 samples. The asymmetric background in the $x = 0$ and 0.04 samples for hole and electron states is strongly reduced in the $x = 0.09$ sample, indicating changes in the band structure for these levels of S substitution. Moreover, it is important to note that the spectra retain the V shape at low energy for all samples studied; therefore, the nodes are not removed by the disorder in the range of S concentration studied [39]. Finally, the main pair of symmetric peaks moves out in energy to ±2.6 meV for the $x = 0.04$ sample, but moves to lower energy in the $x = 0.09$ sample, despite the higher T_c of the latter. The simultaneous occurrence of a decrease in gap and an increase in critical temperature is only possible in a multigap scenario. It may occur with either an increase in interband scattering or a change in the Fermi surface, which alters the ratio of electron and hole states allowing for a merging of the two gaps. This interpretation seems to be consistent with specific heat measurements performed on S-substituted crystals suggesting the merging of gaps with increasing S substitution [40].

The tunneling spectra cannot be adequately reproduced with two gaps models allowing different symmetries of the order parameters including the extended $s_{\pm}$-wave model [10]. The complex multiband structure involves different gaps on different Fermi surface sheets, and there is the possibility that some remain ungapped at temperatures well below T_c [41,42].

IV. IMPURITY BOUND STATES AT DEFECT LOCATIONS

The symmetry of the order parameter has been the subject of intense study in the Fe-based superconductors. Because all five Fe d bands may cross the Fermi level, the number of possible order parameters which can live on these Fermi surfaces is large. Two early papers [10,17] convincingly argued for an $s_{\pm}$-order parameter. In this scenario a spin mediated pairing mechanism would require a sign flip between the phases of the paired carriers, forcing a plus sign on one nested Fermi surface and a minus sign on the other. A combination of several experiments [43,44] conducted on different materials of the Fe-based family supports this picture. However, the FeSe case has challenged this interpretation due to the absence of long range magnetic order. In the superconducting state, the impurities may induce quasiparticle scattering, thereby breaking Cooper pairs and generating a unique pattern of the local density of states. This pattern is dependent on the pairing gap structure. According to Anderson's theorem [45], Cooper pairs with a uniform singlet superconducting gap structure (s wave) can survive in the presence of nonmagnetic impurities, whereas magnetic impurities are very detrimental to superconductivity yielding a unique pattern of the local electronic density of states near an impurity. Theoretically it has been argued that the $s_{\pm}$ pairing, like the d-wave pairing, should be fragile to nonmagnetic impurities [46–51]. In previous STM studies, impurities have been successfully located in iron pnictide superconductors and many interesting features have been reported [43,44]. Our results, shown in Fig. 4, strongly support the sign-reversal gap structure in the FeSe samples, compatible with an $s_{\pm}$- or d-wave order parameter. In Fig. 4(a) an atomically resolved STM image of a defect site (bright spot) is shown. The image has been acquired at a voltage of $V = -10$ mV. Usually these defects, that appear as bright spots, are highly dispersive with energy and they have been observed on samples with $x = 0$, $x = 0.04$, and $x = 0.09$ and they are associated with Se vacancies. Tunneling spectra have been measured at the impurity site and moving away from it along the Fe-Fe bond and Se-Se bond directions

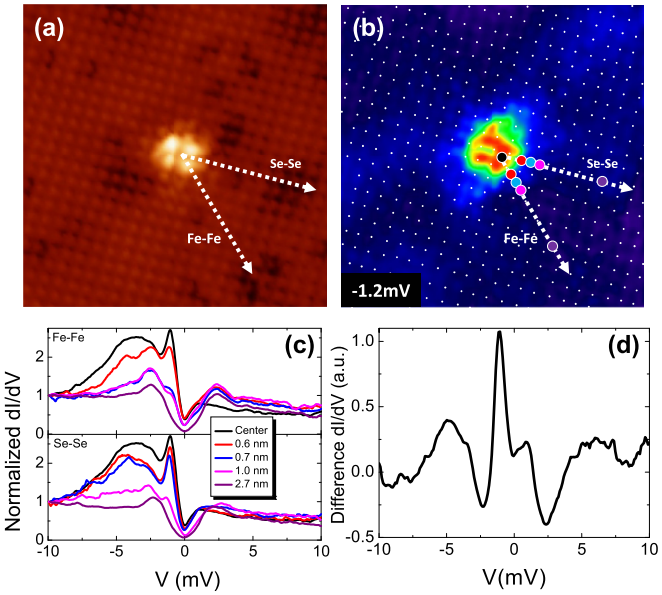

FIG. 4. (Color online) (a) STM topography image acquired on the surface of FeSe single crystal and showing an impurity site. The image has been acquired with a voltage $V = -20$ mV and tunneling current $I = 100$ pA. The scan area is 7.8 nm $\times$ 7.8 nm. (b) Conductance image acquired simultaneously at a voltage $V = -1.2$ mV. White dots in the image correspond to atomic positions of the Se lattice. The two white arrows represent the direction along which tunneling spectra have been acquired. The colored dots show exact locations where the tunneling spectra presented in (c) have been acquired. (c) Sequence of tunneling spectra acquired moving away from the impurity site along the Fe-Fe and Se-Se directions. Tunneling conditions were $V = -10$ mV and $I = 100$ pA. The tunneling spectra have been normalized to the value of conductance at $V = -10$ meV. (d) Difference of the tunneling spectrum measured at the impurity site and the tunneling spectrum measured 2.7 nm away from the impurity site along the Fe-Fe direction.

[Fig. 4(c)]. The tunneling spectrum acquired at the impurity site is strongly asymmetric and presents an impurity state at -1.2 mV. This impurity state is suppressed while moving away on a distance on the order of 10 nm in different directions with slight difference in intensity and decay. This can better be seen in the conductance map acquired simultaneously with the topography image [Fig. 4(b)].

By subtracting the tunneling spectra measured far away from the impurity site from that acquired at the impurity site one can clearly see that the difference of the spectra exhibits a huge asymmetric peak within the superconducting gap [Fig. 4(d)]. It is interesting to mention that in previous experiments on conventional superconductors [52,53], the magnetic impurities give a very similar effect. Here we observe such a peak with a nonmagnetic impurity, which indicates that there should be a sign reversal on the superconducting gap. We observed similar spectra and density of states maps on samples with $x = 0.04$ and $x = 0.09$.

V. VORTEX CORE

When a magnetic field is applied parallel to the c axis of the FeSe sample surface, the field can enter the superconductor in the form of vortices. STM allows for the visualization of the vortex lattice at different magnetic fields by spatially mapping the differential tunneling conductance, which is proportional to the electronic local density of states close to the Fermi level.

Tunneling spectra acquired across the vortex core, as shown in Figs. 5(d), 5(e), and 5(f), reveal the presence of a peak in the density of states at zero energy (Fermi level) at the vortex center, which is a signature of low-lying excitations localized there [54,55]. These states are similar to ballistic Andreev trajectories in short superconductor-normal-superconductor junctions. However, in dirty superconductors, where the superconducting coherence length is much larger than the mean free path $\xi \gg l$, these trajectories mix and one recovers a flat density of states in the vortex core [56]. The presence of a bound state at the vortex center suggests that all crystals studied ($x = 0$, $x = 0.04$, and $x = 0.09$) are in the clean limit ($\xi < l$). Mean free path l can be estimated only roughly due to the multiband nature of this material and the warping of the Fermi sheets. For FeSe single crystals, estimates from Shubnikov–de Haas oscillation measurements yield to values of 30 nm and 80 nm on different Fermi sheets [27], which are much larger than the "averaged" in-plane coherence length $\xi_{ab} \approx 5$ nm obtained from the upper critical field $H_{c2} \approx 12.8$ T [40], confirming the clean limit for this material.

Vortices can be imaged with STM by acquiring the zero bias voltage of the tunneling spectrum as a function of the position in applied magnetic field. Figures 5(a), 5(b), and 5(c) show the zero bias maps for $FeSe_{1-x}S_x$ with $x = 0$, $x = 0.04$, and $x = 0.09$, respectively.

Anisotropic vortex cores, significantly distorted along one of the Fe-Fe bond directions, have been reported in the case of FeSe thin films and single crystals [5,34]. Theoretical models accounting for the vortex shape include superconducting gap anisotropy [57,58] as well as Fermi surface anisotropy [59–61].

In general, the spatial decay of the vortex core states happens on the length scale of $\xi_{BCS} = \hbar v_f/\pi\Delta$, where $\hbar$ is the reduced Planck constant, v_F is the Fermi velocity, and Δ is the gap amplitude. Therefore, in the case of an anisotropic gap where $\Delta(\hat{\mathbf{k}}) \neq$ const, the vortex shape in real space is directly influenced by this anisotropy and in particular the vortex extends in the directions of gap minima or nodes. However, the directional dependence of $v_F(\hat{\mathbf{k}})$ also affects the vortex core shape, especially when combined with a multiband Fermi surface. It has been proven that in the case of Fe-based superconductors, in the absence of strong nodes, the Fermi velocity anisotropy can dominate the decay of vortex core states [62]. This has been confirmed experimentally in the case of LiFeAs, where the shape of the vortex core observed by STM [63] is in contradiction with the superconducting gap minima detected clearly by ARPES [64,65].

In the case of FeSe two papers have studied theoretically the interplay between superconductivity and nematic order with a two band model by solving the Bogoliubov–de Gennes equations [6] and with a Ginzburg-Landau approach [7]. They both found that nematic order can be strongly enhanced in the vortex core and, as a result, the vortex cores become elliptical in shape. Although the elliptical shape of the vortex core could reflect a twofold symmetry of the gap, the authors also found that for an extended $s_{\pm}$-wave state, the gap anisotropy alone without an anisotropy of the Fermi surface would not

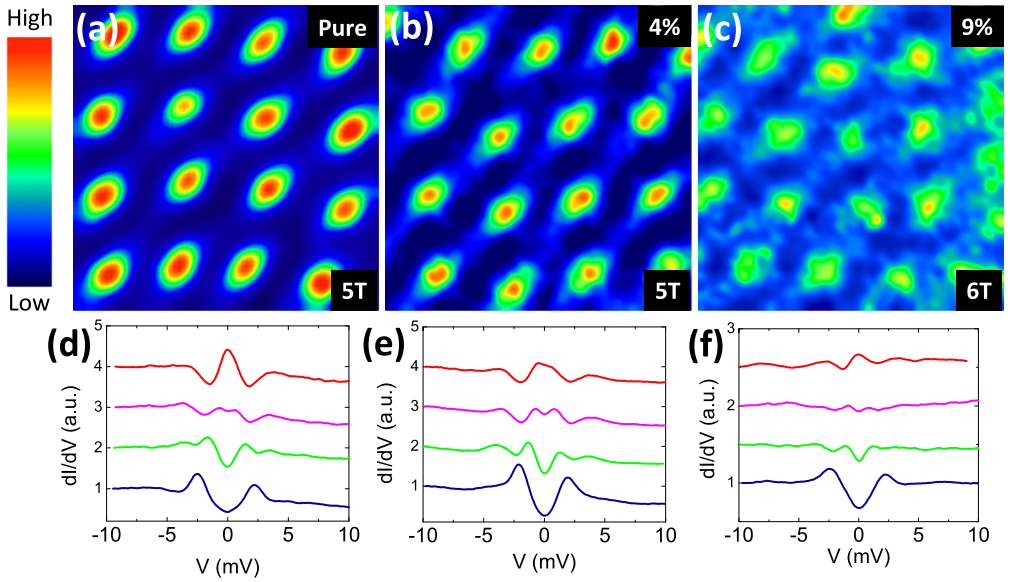

FIG. 5. (Color online) (a)–(c) Zero-bias conductance images at 1.5 K showing vortices. A magnetic field was applied along the c axis. (d)–(f) Characteristic differential conductance spectra (dI/dV) in the mixed state at various positions of the vortex cores, along the Fe-Fe bond direction (corresponding to the long axis of the elliptical core). The line color of the dI/dV corresponds roughly to the positions where the curve was acquired with respect to the conductance image (i.e., red dI/dV curve is red region in conductance image). The tip was stabilized at $V = -10$ mV and $I = 100$ pA. A bias modulation amplitude $V_{\text{mod}} = 0.2$ mV was used. The scan area in all images is 78.1 nm × 78.1 nm (a),(d) $FeSe_{1-\delta}$ (b),(e) $FeSe_{1-x}S_x$ with $x = 0.04$, and (c),(f) $FeSe_{1-x}S_x$ with $x = 0.09$.

reproduce the observed shape of the vortex core in FeSe. Therefore, we conclude that the observed elliptical shape is quite likely reflecting the Fermi surface anisotropy in this system.

We found that upon S substitution the vortex core becomes more isotropic, as shown in Fig. 5(c). Analysis of the STM vortex images yields $(L_{\text{long}} - L_{\text{short}})/L_{\text{short}} = 0.5 \pm 0.1, 0.4 \pm 0.1, 0.2 \pm 0.1$ (where L_{long} and L_{short} are the major and the minor axes of the elliptical vortex core) for the samples with $x = 0$, $x = 0.04$, and $x = 0.09$, respectively. The vortex anisotropy that we observe is in quantitative agreement with the Fermi surface distortions reported from ARPES measurements on S-substituted single crystals [26]. While the microscopic origin of the nemacity in FeSe is still under debate, our measurements suggest that the changes in Fermi surface upon S substitution and the scattering associated with the disorder might reduce the nematic order.

VI. CONCLUSIONS

In summary, our low temperature scanning tunneling microscopy and spectroscopy study of $FeSe_{1-x}S_x$ single crystals shows that the increase in the superconducting critical temperature in the 9% S-substituted samples is accompanied with a decrease in the energy position of the main coherence peaks observed in the tunneling spectra. A decrease in the gap occurring simultaneously with an increase in T_c can be explained in terms of an increase of the Fermi surface pocket corresponding to the gap probed by c-axis tunneling (Γ band) and/or an increase of interband scattering which induces a merging of gaps in a multiband system. Most importantly, a signature of nematicity in FeSe is the elliptical shape of the Abrikosov vortex cores in the superconducting state. Our results show that the elliptical shaped cores become more isotropic in the 9% S-substituted sample suggesting that the Fermi surface is less anisotropic. These results seem to be in agreement with a recent angle-resolved photoemission spectroscopy study of $FeSe_{1-x}S_x$ single crystals [26], in which the authors correlate the decrease of the structural transition temperature T_s with a decrease in the orbital ordering. STM tunneling spectra in the superconducting state, on the other hand, are clearly V-shaped at low energy around the Fermi level and in-gap quasiparticle excitations at nonmagnetic impurity sites are consistent with sign changes of the superconducting order parameter. Therefore, this suggests that, while interactions favoring orbital ordering dominate near T_s, magnetic fluctuations may still assist the superconducting pairing.

ACKNOWLEDGMENTS

The authors would like to acknowledge fruitful discussions with John Zasadzinski, Igor Mazin and Alexander Kordyuk. This work at Temple University, where low temperature scanning tunneling measurements were performed, was supported by the U.S. Department of Energy, Office of Basic Energy Sciences, Division of Materials Sciences and Engineering under Award DE-SC0004556. The work at Drexel University and at the M.V. Lomonosov Moscow State University was supported by Award No. FSAX-14-60108-0, OISE-14-60109-0 of the U.S, Civilian Research and Development Foundation (CRDF). The work in Russia was supported in part from the Ministry of Education and Science of the Russian Federation in the framework of Increase Competitiveness Program of NUST "MISiS" (Grant No. K4-2015-020). One of the authors (C.D.G.) would like to acknowledge partial support from MIUR (Ministry of Education, Universities and Research of the Italian Government).

[1] T. M. McQueen, A. J. Williams, P. W. Stephens, J. Tao, Y. Zhu, V. Ksenofontov, F. Casper, C. Felser, and R. J. Cava, Phys. Rev. Lett. **103**, 057002 (2009).

[2] M. D. Watson *et al.*, Phys. Rev. B **91**, 155106 (2015).

[3] R. M. Fernandes, A. V. Chubukov, and J. Schmalian, Nat. Phys. **10**, 97 (2014).

[4] F. C. Hsu *et al.*, Proc. Natl. Acad. Sci. USA **105**, 14262 (2008).

[5] C. L. Song *et al.*, Science **332**, 1410 (2011).

[6] H. H. Hung, C. L. Song, X. Chen, X. Ma, Q. K. Xue, and C. Wu, Phys. Rev. B **85**, 104510 (2012).

[7] D. Chowdhury, E. Berg, and S. Sachdev, Phys. Rev. B **84**, 205113 (2011).

[8] H. Kontani and S. Onari, Phys. Rev. Lett. **104**, 157001 (2010).

[9] Y. Yanagi, Y. Yamakawa, and Y. Ōno, Phys. Rev. B **81**, 054518 (2010).

[10] I. I. Mazin, D. J. Singh, M. D. Johannes, and M. H. Du, Phys. Rev. Lett. **101**, 057003 (2008).

[11] A. V. Chubukov, R. M. Fernandes, and J. Schmalian, Phys. Rev. B **91**, 201105 (2015).

[12] R. M. Fernandes, A. V. Chubukov, J. Knolle, I. Eremin, and J. Schmalian, Phys. Rev. B **85**, 024534 (2012).

[13] C. Xu, M. Müller, and S. Sachdev, Phys. Rev. B **78**, 020501 (2008).

[14] F. Krüger, S. Kumar, J. Zaanen, and J. van den Brink, Phys. Rev. B **79**, 054504 (2009).

[15] P. Dai, J. Hu, and E. Dagotto, Nat. Phys. **8**, 709 (2012).

[16] S. Onari and H. Kontani, Phys. Rev. Lett. **109**, 137001 (2012).

[17] K. Kuroki, S. Onari, R. Arita, H. Usui, Y. Tanaka, H. Kontani, and H. Aoki, Phys. Rev. Lett. **101**, 087004 (2008).

[18] J. H. Chu, H. H. Kuo, J. G. Analytis, and I. R. Fisher, Science **337**, 710 (2012).

[19] H. H. Kuo, M. C. Shapiro, S. C. Riggs, and I. R. Fisher, Phys. Rev. B **88**, 085113 (2013).

[20] K. Nakayama, Y. Miyata, G. N. Phan, T. Sato, Y. Tanabe, T. Urata, K. Tanigaki, and T. Takahashi, Phys. Rev. Lett. **113**, 237001 (2014).

[21] T. Shimojima *et al.*, Phys. Rev. B **90**, 121111 (2014).

[22] D. Chareev, E. Osadchii, T. Kuzmicheva, J. Y. Lin, S. Kuzmichev, O. Volkova, and A. Vasiliev, CrystEngComm **15**, 1989 (2013).

[23] M. Ma, D. Yuan, Y. Wu, H. Zhou, X. Dong, and F. Zhou, Supercond. Sci. Technol. **27**, 122001 (2014).

[24] Q. Wang *et al.*, arXiv:1502.07544 [Nature Materials (to be published)].

[25] J. Maletz *et al.*, Phys. Rev. B **89**, 220506 (2014).

[26] M. D. Watson, T. K. Kim, A. A. Haghighirad, S. F. Blake, N. R. Davies, M. Hoesch, T. Wolf, and A. I. Coldea, Phys. Rev. B **92**, 121108 (2015).

[27] T. Terashima *et al.*, Phys. Rev. B **90**, 144517 (2014).

[28] S. Kasahara, T. Watashige, T. Hanaguri, Y. Kohsaka, T. Yamashita, Y. Shimoyama, Y. Mizukami, R. Endo, H. Ikeda, K. Aoyama, T. Terashima, S. Uji, T. Wolf, H. v. Löhneysen, T. Shibauchi, and Y. Matsuda, Proc. Natl. Acad. Sci. USA **111**, 16309 (2014).

[29] E. Venzmer, A. Kronenberg, and M. Jourdan, arXiv:1506.01877v1.

[30] Y. G. Ponomarev *et al.*, J. Supercond. Nov. Magn. **26**, 2867 (2013).

[31] J. Y. Lin, Y. S. Hsieh, D. A. Chareev, A. N. Vasiliev, Y. Parsons, and H. D. Yang, Phys. Rev. B **84**, 220507 (2011).

[32] C.-L. Song, Y.-L. Wang, Y.-P. Jiang, L. Wang, K. He, X. Chen, J. E. Hoffman, X.-C. Ma, and Q.-K. Xue, Phys. Rev. Lett. **109**, 137004 (2012).

[33] S. Knöner, D. Zielke, S. Köhler, B. Wolf, T. Wolf, L. Wang, A. Böhmer, C. Meingast, and M. Lang, Phys. Rev. B **91**, 174510 (2015).

[34] T. Watashige *et al.*, Phys. Rev. X **5**, 031022 (2015).

[35] J. Tersoff and D. R. Hamann, Phys. Rev. Lett. **50**, 1998 (1983).

[36] W. C. Lee and C. Wu, Phys. Rev. Lett. **103**, 176101 (2009).

[37] A. A. Golubov and I. I. Mazin, Appl. Phys. Lett. **102**, 032601 (2013).

[38] E. L. Wolf, *Principles of Electron Tunneling Spectroscopy: Second Edition* (Oxford Scholarship Online, Oxford, 2011).

[39] V. Mishra, G. Boyd, S. Graser, T. Maier, P. J. Hirschfeld, and D. J. Scalapino, Phys. Rev. B **79**, 094512 (2009).

[40] M. Abdel-Hafiez *et al.*, Phys. Rev. B **91**, 165109 (2015).

[41] L. Komendová, Y. Chen, A. A. Shanenko, M. V. Milošević, and F. M. Peeters, Phys. Rev. Lett. **108**, 207002 (2012).

[42] R. Khasanov, M. Bendele, A. Amato, K. Conder, H. Keller, H. H. Klauss, H. Luetkens, and E. Pomjakushina, Phys. Rev. Lett. **104**, 087004 (2010).

[43] J. E. Hoffman, Rep. Prog. Phys. **74**, 124513 (2011).

[44] H. Yang, Z. Wang, D. Fang, Q. Deng, Q. H. Wang, Y. Y. Xiang, Y. Yang, and H. H. Wen, Nat. Commun. **4**, 2749 (2013).

[45] P. W. Anderson, J. Phys. Chem. Solids **11**, 26 (1959).

[46] S. Onari and H. Kontani, Phys. Rev. Lett. **103**, 177001 (2009).

[47] T. Kariyado and M. Ogata, J. Phys. Soc. Jpn. **79**, 083704 (2010).

[48] Y. Bang, H. Y. Choi, and H. Won, Phys. Rev. B **79**, 054529 (2009).

[49] A. F. Kemper, C. Cao, P. J. Hirschfeld, and H. P. Cheng, Phys. Rev. B **80**, 104511 (2009).

[50] K. Nakamura, R. Arita, and H. Ikeda, Phys. Rev. B **83**, 144512 (2011).

[51] P. J. Hirschfeld, M. M. Korshunov, and I. I. Mazin, Rep. Prog. Phys. **74**, 124508 (2011).

[52] A. Yazdani, B. A. Jones, C. P. Lutz, M. F. Crommie, and D. M. Eigler, Science **275**, 1767 (1997).

[53] M. Iavarone, G. Karapetrov, J. Fedor, D. Rosenmann, T. Nishizaki, and N. Kobayashi, J. Phys.: Condens. Matter **22**, 015501 (2010).

[54] C. Caroli, P. G. De Gennes, and J. Matricon, Phys. Lett. **9**, 307 (1964).

[55] H. F. Hess, R. B. Robinson, R. C. Dynes, J. M. Valles, Jr., and J. V. Waszczak, Phys. Rev. Lett. **62**, 214 (1989).

[56] C. Renner, A. D. Kent, P. Niedermann, Ø. Fischer, and F. Lèvy, Phys. Rev. Lett. **67**, 1650 (1991).

[57] N. Hayashi, M. Ichioka, and K. Machida, Phys. Rev. Lett. **77**, 4074 (1996).

[58] N. Hayashi, M. Ichioka, and K. Machida, Phys. Rev. B **56**, 9052 (1997).

[59] F. Gygi and M. Schlüter, Phys. Rev. Lett. **65**, 1820 (1990).

[60] F. Gygi and M. Schlüter, Phys. Rev. B **43**, 7609 (1991).

[61] Y. D. Zhu, F. C. Zhang, and M. Sigrist, Phys. Rev. B **51**, 1105 (1995).

[62] Y. Wang, P. J. Hirschfeld, and I. Vekhter, Phys. Rev. B **85**, 020506 (2012).

[63] T. Hanaguri, K. Kitagawa, K. Matsubayashi, Y. Mazaki, Y. Uwatoko, and H. Takagi, Phys. Rev. B **85**, 214505 (2012).

[64] K. Umezawa, Y. Li, H. Miao, K. Nakayama, Z. H. Liu, P. Richard, T. Sato, J. B. He, D. M. Wang, G. F. Chen, H. Ding, T. Takahashi, and S. C. Wang, Phys. Rev. Lett. **108**, 037002 (2012).

[65] S. V. Borisenko, V. B. Zabolotnyy, A. A. Kordyuk, D. V. Evtushinsky, T. K. Kim, I. V. Morozov, R. Follath, and B. Büchner, Symmetry **4**, 251 (2012).